

Galactic cosmic ray transport in the absence of resonant scattering

O. Pezzi  ¹  and P. Blasi  ^{2,3}

¹ Istituto per la Scienza e Tecnologia dei Plasmi, Consiglio Nazionale delle Ricerche, Via Amendola 122/D, I-70126 Bari, Italy

² Gran Sasso Science Institute, Viale F. Crispi 7, I-67100 L’Aquila, Italy

³ INFN/Laboratori Nazionali del Gran Sasso, Via G. Acitelli 22, I-67100 Assergi (AQ), Italy

Accepted XXX. Received YYY; in original form ZZZ

ABSTRACT

Galactic cosmic ray transport relies on the existence of turbulence on scales comparable with the gyration radius of the particles and with wavenumber vector oriented along the local magnetic field. In the standard picture, in which turbulence is injected at large scales and cascades down to smaller scales, it is all but guaranteed that turbulence on the relevant scales may be present, either because of anisotropic cascading or because of the onset of damping processes. This raises questions on the nature of cosmic-ray scattering, especially at energies $\gtrsim 1$ TeV, where self-generation is hardly relevant. Here, by means of numerical simulations of charged test-particles in a prescribed magnetic field, we investigate particle diffusion in a situation in which turbulence is mainly present at large scales, with the possible presence of a smaller power on small scales, and discuss possible implications of this setup for cosmic-ray transport phenomenology.

Key words: (ISM:) cosmic rays – turbulence – diffusion

1 INTRODUCTION

The simplest description of cosmic ray (CR) transport in the Galaxy relies on the existence of possibly-broadened resonances between particle gyration and $1/k$, k being the wavenumber of turbulent fluctuations. At first glance, the approximately power-law-like shape of the CR energy spectrum over many decades well reconciles with the power-law turbulent spectrum in k -space, as turbulence is injected on large scales and eventually cascades to smaller spatial scales.

This simple picture has been recently challenged based on both observational and theoretical considerations. The AMS-02 measurements identified a spectral hardening at rigidity $\sim 200 - 300$ GV in the spectrum of CR protons (Choutko 2016), helium (Aguilar et al. 2015), and heavier nuclei (Aguilar et al. 2017). This feature was also observed in the secondary to primary ratios, such as B/C and B/O (Aguilar et al. 2016), thus strongly suggesting that the slope change is due to a variation of the diffusive properties of CRs in the Galaxy at the same rigidity (Génolini et al. 2017; Evoli et al. 2020). This finding indicates that either the scattering properties or the nature of turbulence change at ~ 200 GV. The spectral hardening has been associated with either a non-separable spatial dependence of the diffusion coefficient in the Galaxy (Tomassetti 2012) or the transition from self-generated to pre-existing turbulence (Blasi et al. 2012). In particular, the CR self-generation of scattering centers is expected to be efficient at low energies (below a few hundred GV) (Kulsrud & Pearce 1969; Skilling 1975; Holmes & Sciama 1975), while at higher energies the process becomes ineffective and the turbulence responsible for particle scattering must have another origin, e.g., pre-existing Galactic turbulence perhaps injected through supernova explosions on large scales and cascading down to smaller spatial scales (Blasi et al. 2012; Amato & Blasi 2018).

In this simple scenario, the match between the two regimes naturally occurs in the few hundred GV rigidity range, if the cascade is assumed to be isotropic in k space (Zhou & Matthaeus 1990). This latter assumption is however at odds with the spectral anisotropy of Alfvénic turbulence (Shebalin et al. 1983; Sridhar & Goldreich 1994; Goldreich & Sridhar 1995; Matthaeus et al. 1996, 2012; Oughton & Matthaeus 2020; Schekochihin 2022). Indeed, most of the turbulent power is efficiently transferred to smaller scales in the directions perpendicular to the magnetic field rather than in the parallel direction, and the pitch-angle diffusion coefficient decreases as a result of this effect (Chandran 2000). Hence, the issue of understanding the origin of the CR scattering at high energies remains open.

Magnetosonic fluctuations have also been considered in this context (Cho & Lazarian 2002; Cho et al. 2002). The CR spatial diffusion coefficients are usually calculated by computing the pitch-angle diffusion coefficient $D_{\mu\mu}$ in such a turbulence under quasi-linear/weakly-nonlinear frameworks (Völk 1973; Chandran 2000; Yan & Lazarian 2002, 2008; Fornieri et al. 2021), and then deriving the corresponding spatial diffusion coefficient. However, magnetosonic modes have their own problematic aspects. Slow magnetosonic fluctuations cascade anisotropically in k -space, similar to Alfvénic turbulence. The cascade of fast magnetosonic modes is isotropic, but their spectrum is affected by various damping mechanisms, whose relevance critically depends on the medium properties, such as the plasma β . In fact, in older literature fast modes were never included in the discussion of CR diffusion since they were expected to be heavily damped (Barnes 1966). By investigating the transition between self-generated and pre-existing turbulence, Kempinski & Quataert (2022) have recently concluded that the shape of the transition depends upon details, and a fine tuning is often necessary to reconcile results with observations of secondary to primary ratios. The authors also suggested that fast magnetosonic modes may develop shocklets, thus leading to unusual

* E-mail: oreste.pezzi@istp.cnr.it

scattering properties. Again, the issue of CR scattering for particles with energy \gtrsim TeV appears all but clear.

Aside from these approaches, the spatial diffusion coefficient has also been computed numerically by propagating charged test-particles in synthetic models of turbulence either generated on grid (De Marco et al. 2007; Dundovic et al. 2020; Reichherzer et al. 2022; Kuhlen et al. 2022) or built as a superposition of plane waves (Casse et al. 2001; Pucci et al. 2016; Mertsch 2020). Most notably, there have been attempts at obtaining clues on CR transport by directly propagating particles in magnetohydrodynamic (MHD) simulated turbulence (Cohet & Marcowith 2016; Pezzi et al. 2022). This latter approach may appear as the most appropriate for assessing the role of different MHD modes. However, the dynamical range achieved in MHD simulations is typically rather small, covering only about 3 decades in k -space, of which only one and a half below the energy containing scale. This limitation sets a correspondingly small energy range for which CR transport is properly described. Such a dynamical range is too small to explore to its full extent the anisotropic cascade of Alfvénic and slow magnetosonic modes. As a result, the spatial diffusion coefficients derived within this approach are very similar to those naively obtained in quasi-linear theory (for parallel diffusion) or calculated numerically with synthetic isotropic turbulence (see, e.g., Cohet & Marcowith (2016); Pezzi et al. (2022)).

The confusing situation illustrated above becomes even more puzzling if one recalls that Galactic CRs spend most of their confinement time in the Galactic halo, where little fresh injection of turbulence on large scales is expected. The halo turbulence should most likely originate in the disc region and eventually be advected into the halo while cascading from the injection scale L to smaller scales, on times of the order of $L/v_A \sim$ few million years. This time scale is rather close to the confinement time of high energy CRs and it is not guaranteed that the cascade may develop completely.

All these concerns have motivated the *gedankenexperiment* underlying the present work. Our goal is to investigate the transport of particles in the Galaxy in a scenario in which the turbulent cascade does not develop or develops partially, so that most of the power remains in a narrow neighborhood of the coherence scale l_c and little power is available for resonant scattering at scales $< l_c$. At variance with much previous literature, we do not focus only on the calculation of diffusion coefficients but we also discuss the problem in terms of CR confinement time in the Galaxy. In the absence of turbulent cascade, particle transport is dominated by the random walk of magnetic field lines (FLRW). FLRW has been extensively studied to determine the magnetic field topology and point out potential regions of trapping (Chuaychai et al. 2007; Sonsrettee et al. 2016). Its effects on particle diffusion and, more specifically, on the transport of Galactic CRs have been so far poorly investigated (see however Kuhlen et al. (2022)). One can picture the magnetic field configuration when turbulence is concentrated in a narrow k -space region as a coherent field whose orientation changes in cells of size $\sim l_c$. In the community involved in the investigation of the Galactic magnetic field through Faraday rotation measures, this would correspond to the *ordered field* (Ferrière 2020), while the denomination *turbulent field* is limited to smaller-scale fluctuations.

Here, we construct the magnetic field on a three-dimensional (3D) grid and we propagate charged test particles in such a grid by changing the power in the form of large-scale coherent field with respect to the one going into the standard turbulent component, thus modulating the role of FLRW. For standard values of the parameters appropriate to the interstellar medium, $l_c \sim 10$ pc and the energy of particles that would resonate with such perturbations is $E(l_c) \simeq 10$ PeV in a magnetic field $\sim 1 \mu\text{G}$. In the absence of turbulent cascading, lower energy

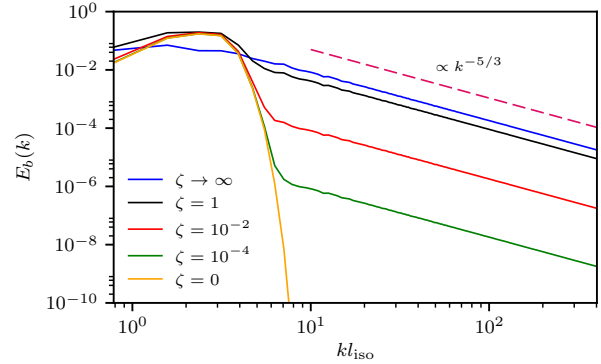


Figure 1. Omni-directional spectrum of the magnetic field energy, $E_b(k)$, for several values of ζ : $\zeta \rightarrow \infty$ (blue), $\zeta = 1$ (black), $\zeta = 10^{-2}$ (red), $\zeta = 10^{-4}$ (green), and $\zeta = 0$ (orange). The cerise-red dashed line displays the Kolmogorov $k^{-5/3}$ slope for reference.

particles would not diffuse resonantly in the volume of the Galaxy but rather follow magnetic field lines in their random wandering.

2 NUMERICAL METHOD AND SETUPS

We follow the trajectories of $N_p = 8192$ relativistic test protons in a non-relativistic magnetostatic turbulence ($\partial\mathbf{B}/\partial t = 0$, $\mathbf{E} = 0$) in the absence of background field, $\langle \mathbf{B} \rangle = 0$ being $\langle \dots \rangle$ here the average on the computational box. The motion equations are:

$$\begin{aligned} \frac{d\mathbf{r}}{dt} &= \mathbf{v} \\ \frac{d\mathbf{p}}{dt} &= e \frac{\mathbf{v}}{c} \times \delta\mathbf{B}(\mathbf{r}), \end{aligned} \quad (1)$$

being e the proton charge and c the speed of light. Particle position, speed, momentum, and Lorentz factor are respectively indicated by \mathbf{r} , \mathbf{v} , $\mathbf{p} = m_p \gamma \mathbf{v}$, and $\gamma = \sqrt{1 + \mathbf{p}^2/m_p^2 c^2}$, being m_p the proton mass. The purely-fluctuating magnetic field $\delta\mathbf{B}(\mathbf{r})$, with r.m.s. amplitude $\delta B_{\text{rms}} = \sqrt{\langle \delta\mathbf{B}^2 \rangle}$, is split as $\delta\mathbf{B}(\mathbf{r}) = \delta\mathbf{B}_{\text{res}}(\mathbf{r}) + \delta\mathbf{B}_{\text{coh}}(\mathbf{r})$, being $\langle \delta\mathbf{B}_{\text{res}} \rangle = \langle \delta\mathbf{B}_{\text{coh}} \rangle = 0$, while their r.m.s. amplitudes satisfy $\delta B_{\text{rms}}^2 = \delta B_{\text{res}}^2 + \delta B_{\text{coh}}^2 = 1 \mu\text{G}$. $\delta\mathbf{B}_{\text{res}}(\mathbf{r})$ is the pure turbulent component modeled here with a Kolmogorov-like spectrum and responsible for resonant scattering of lower energy particles. $\delta\mathbf{B}_{\text{coh}}(\mathbf{r})$ mimics the large-scale complexity of the magnetic field responsible for FLRW.

The spectrum function $S(k) = S^{\text{res}}(k) + S^{\text{coh}}(k)$, associated with $\delta\mathbf{B}(\mathbf{r})$, is composed of:

$$\begin{aligned} S^{\text{res}}(k) &= \delta B_{\text{res}}^2 \frac{C(q=4, s)}{\pi k^2} l_{\text{iso}} \frac{(kl_{\text{iso}})^4}{\left(1 + k^2 l_{\text{iso}}^2\right)^{s/2+2}}, \\ S^{\text{coh}}(k) &= \delta B_{\text{coh}}^2 \frac{D(k^*, \Delta k^*)}{(2\pi)^{3/2} \Delta k^3} \exp\left[-\frac{1}{2} \left(\frac{k - k^*}{\Delta k^*}\right)^2\right]. \end{aligned} \quad (2)$$

In the expression for $S^{\text{res}}(k)$, the bend-over scale l_{iso} is the scale at which the inertial range of turbulence, whose slope is controlled by the parameter s , begins. Here, we set $L_{\text{box}}/l_{\text{iso}} = 8$ to include several correlation lengths in the box, being $L_{\text{box}} = 512$ pc and $s = 5/3$ (Kolmogorov turbulence). The normalization constant $C(q, s)$ is set as to ensure that the energy density is normalized to δB_{res}^2 , i.e., $\delta B_{\text{res}}^2 = 4\pi \int_0^\infty dk k^2 S^{\text{res}}(k)$ (Sonsrettee et al. 2015), with $q = 4$ to achieve homogeneity of turbulent fluctuations (Batchelor 1982) (see Dundovic et al. (2020) for additional details).

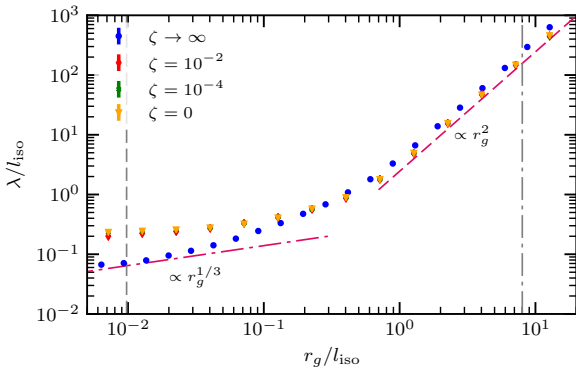


Figure 2. Isotropic mean free path $\lambda = 3D_{\text{iso}}/c$ as a function of the particle gyroradius r_g , for $\zeta \rightarrow \infty$ (blue dots), $\zeta = 10^{-2}$ (red rhombuses), $\zeta = 10^{-4}$ (green crosses), and $\zeta = 0$ (orange triangles). Cerise-red lines respectively display the $r_g^{1/3}$ dependence (dot-dashed) and the r_g^2 dependence (dashed). Gray vertical lines indicate the gyroradius at which resonance is lost for numerical reasons (dashed) and corresponding to the box size $r_g = L_{\text{box}}$ (dot-dashed), respectively.

$S^{\text{coh}}(k)$ is taken as a Gaussian bump in k -space centered at $k = k^* = 2/l_{\text{iso}}$ with width $\Delta k^* = \pi/(4l_{\text{iso}})$. By normalizing the energy density to δB_{coh}^2 , one finds $D(k^*, \Delta k^*) = \Delta k^{*2} / \left(k^{*2} + \Delta k^{*2} + 2\sqrt{\frac{2}{\pi}} k^* \Delta k^* \right)$.

With the spectral function $S(k)$ in Eqs. (2), the correlation length of magnetic field fluctuations is (Sonsrettee et al. 2015):

$$l_c = \frac{\pi}{2} \frac{\int_0^\infty dk k S(k)}{\int_0^\infty dk k^2 S(k)} = l_{\text{iso}} \frac{2\pi}{1+\zeta} \left[\zeta \frac{2C(q=4, s)}{s(s+2)} + \frac{D(k^*, \Delta k^*)}{2\sqrt{2\pi}} \cdot \frac{\Delta k^* + k^* \sqrt{\frac{\pi}{2}}}{l_{\text{iso}} \Delta k^{*2}} \right], \quad (3)$$

where $\zeta = \delta B_{\text{res}}^2 / \delta B_{\text{coh}}^2$. With our choice of the parameters l_{iso} , k^* , and Δk^* , $l_c \simeq 0.5/l_{\text{iso}} = 32\text{pc}$ for different values of ζ . Such a correlation length corresponds to a particle energy $E(l_c) \simeq 30\text{PeV}$.

The different role of $\delta \mathbf{B}_{\text{res}}(\mathbf{r})$ and $\delta \mathbf{B}_{\text{coh}}(\mathbf{r})$ can be appreciated from Figure 1 that displays the magnetic field omni-directional energy spectrum $E_b(k)$ for different values of ζ . As ζ decreases, less power is available for resonant scattering and goes into the coherent field component. The case $\zeta \rightarrow \infty$ corresponds to the one explored by Dundovic et al. (2020) as the power is entirely associated to a Kolmogorov-like turbulent component. In turn, the case $\zeta = 0$ implies that all power is contained in a coherent field that changes direction on a scale $\sim 1/k^* \sim l_c$.

Magnetic fluctuations are generated on a tri-periodic cubic grid of size L_{box} discretized with $N = 1024$ grid points in each direction, with double-precision floating point. The spectral tensor of the magnetic fluctuations is assigned in the wavenumber space that is limited, in each direction, by $k_{\text{min}} = k_0 = 2\pi/L_{\text{box}} = \pi/4l_{\text{iso}}$ and the Nyquist wave number $k_{\text{max}} = k_0(N/2-1)$, following the procedure proposed by Sonsrettee et al. (2015) which fulfills $\nabla \cdot \delta \mathbf{B}(\mathbf{r}) = 0$. Particle trajectories are obtained by integrating Eqs. (1) with the symplectic Boris method, where tri-linear interpolation method is adopted to evaluate the magnetic field at the particle position. For one set of parameters, the integration is repeated for an ensemble of N_p particles in a single realization of the magnetic field (see also Dundovic et al. (2020)).

3 SIMULATION RESULTS

An extensive numerical campaign has been conducted to tackle the following two scientific questions.

How do particles diffuse in the absence of turbulence at resonant scales? We carried out a series of simulations in which we change the value of ζ . For each value of ζ we performed several runs at different particle gyroradius in the range $r_g/l_{\text{iso}} \in [10^{-2}, 10^1]$, i.e., $E_{\text{Pev}} \in [0.6, 6 \times 10^2]$. Particles are injected homogeneously throughout the box with speed directions sampled uniformly on the 3D sphere. Given the grid size of 1024^3 , the chosen gyroradius range guarantees to describe particle scattering in about one energy decade in the inertial range of turbulence and to recover the high-energy transition occurring at scales about $r_g \sim l_c$ (Subedi et al. 2017; Dundovic et al. 2020). For each run, we calculated the spatial diffusion coefficient along each direction, e.g., D_{xx} , from the time-dependent diffusion coefficients $D_{\text{xx}}^{\text{run}}(t) = \langle (\Delta x(t))^2 \rangle / 2t$, being $\Delta x(t)$ the particle displacement during a time interval t and $\langle \dots \rangle$ indicating hereafter the average on the particle ensemble. D_{xx} is the long-time limit of $D_{\text{xx}}^{\text{run}}(t)$ when it has reached the diffusive plateau. Analogous definitions hold for the y and z directions. For a vanishing regular field, particle diffusion is spatially isotropic and the particle mean free path is $\lambda = 3D_{\text{iso}}/c$, being $D_{\text{iso}} = (D_{\text{xx}} + D_{\text{yy}} + D_{\text{zz}})/3$ the isotropic diffusion coefficient.

Figure 2 shows the mean free path λ as a function of the particle gyroradius r_g for $\zeta \rightarrow \infty$ (blue dots), $\zeta = 10^{-2}$ (red rhombuses), $\zeta = 10^{-4}$ (green crosses), and $\zeta = 0$ (orange triangles). We disregarded the case $\zeta = 1$ shown in Figure 1 since the magnetic energy spectrum is quite similar to the one achieved in the $\zeta \rightarrow \infty$ case. At high energies, i.e., $r_g/l_{\text{iso}} \gtrsim 1$, the transition to the scaling $\lambda_{\text{iso}} \sim r_g^2$ (cerise-red dashed line in Fig. 2) is recovered for all values of ζ .

In the case $\zeta \rightarrow \infty$, the power spectrum changes continuously in k , namely there is no jump at $k > 1/l_c$. Hence, the corresponding pathlength for particle scattering also changes in a continuous manner with energy and its energy dependence agrees, for gyroradius $r_g < l_c$, with the prediction $\sim r_g^{1/3}$ (cerise-red dot-dashed line in Fig. 2). This is not the case when $\zeta \ll 1$. For particles with energy below E_c , the pathlength due to resonant scattering would become $\gg l_c$, hence the transport is dominated by the FLRW, i.e., the pathlength becomes independent of energy and $\sim l_c$ (recall that $l_c/l_{\text{iso}} \sim 0.5$). This is clear from inspecting the low-energy behaviour of the curves in Figure 2 with $\zeta \ll 1$. We expect that for any value of ζ there should be a sufficiently small energy for which the pathlength due to resonant scattering becomes again smaller than l_c : at such energies one should recover the energy dependent pathlength expected in quasi-linear theory and previously found by (Subedi et al. 2017; Dundovic et al. 2020). Given the dynamical range of our simulations, it is difficult to test this expectation here.

This situation resembles what we expect to happen in presence of self-generation, which produces turbulent power only at large wavenumbers. If we assume, in a very qualitative way, that the diffusion coefficient at $R < TV$ as inferred from secondary to primary ratios is $D(E) \sim 3 \times 10^{28} E_{\text{GeV}}^{1/2} \text{ cm}^2/\text{s}$, then the corresponding pathlength is comparable with $l_c \simeq 32\text{pc}$ (see discussion above) for energies of order $\sim \text{TeV}$, tantalizingly close to the energy where a break is observed in both the spectra of primary nuclei and in the secondary to primary ratios. We stress once more that the transport of high-energy particles on which these considerations are based has been obtained by requiring only that the large-scale magnetic field is randomly oriented on scales $\sim l_c$, hence particle scattering would be guaranteed even in pathological cases in which the Alfvénic turbulence becomes strongly anisotropic or in the presence

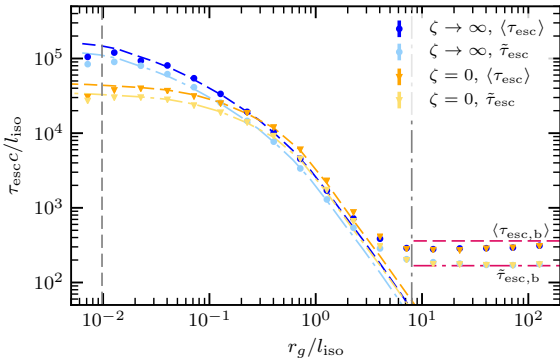


Figure 3. Escape times as a function of the particle gyroradius r_g . Blue (light blue) points indicate respectively the average (median) escape times, computed for the $\zeta \rightarrow \infty$ case. Orange (light orange) triangles refer to the average (median) escape times in the $\zeta = 0$ case. Blue and orange dashed lines indicate the diffusive escape time $\tau_D = L_{\text{esc}}^2/2D_{\text{iso}}$ for the two cases $\zeta \rightarrow \infty$ and $\zeta = 0$. Light blue and orange dot-dashed lines show the prediction $0.75\tau_D$ for the two different setups. The horizontal cerise-red lines correspond to the average ballistic escape time, $\langle \tau_{\text{esc},b} \rangle$ (dashed) and the median ballistic escape time $\tilde{\tau}_{\text{esc},b}$ (dot dashed). Gray vertical lines indicate the gyroradius at which resonance is lost for numerical reasons, i.e. the gyroradius that comprises at least five grid points, (dashed) and corresponding to the box size $r_g = L_{\text{box}}$ (dot-dashed), respectively.

of severe damping of fast magnetosonic modes. This implies that cases where the computed diffusion coefficient is extremely large or shows odds energy dependence (e.g., Fornieri et al. (2021)) may provide unphysical insights since they neglect large-scale FLRW. All these considerations will turn out to be foundational to address the second following question.

What is the confinement time the Galaxy in the absence of turbulent power on resonant scales? In the energy range accessible to our simulations, the diffusion coefficient in the low energy regime is roughly the same for small values of ζ . Hence, we will focus here only on the limit cases $\zeta \rightarrow \infty$ and $\zeta = 0$. For each value of ζ , we performed different runs at different particle gyroradius in the range $r_g/l_{\text{iso}} \in [10^{-2}, 10^2]$, i.e., particle energy $E_{\text{PeV}} \in [0.6, 6 \times 10^3]$ in physical units. We extended this range for about a decade at high energies for recovering the transition to the ballistic transport.

For mimicking the particle escape from the Galactic halo, we identify the (x, y) plane at $z = L_{\text{box}}/2$ as the Galactic disc, while the halo fills the z direction out to an escape boundary at $L_{\text{esc}} = L_{\text{box}}/2 + 10L_{\text{box}}$. Particles are injected isotropically in such an infinitesimally thin disc. A particle is considered as escaped when its displacement along the z direction reaches the threshold height L_{esc} . In order to simulate this situation, we use periodic boundary conditions on the individual box, while keeping track on the displacement in the z direction. At the end of each run, all particles escape. Due to the randomness of the magnetic field perturbations, the probability distribution function (PDF) of the escape times is wide (not shown here), thus indicating that particles escape with different times τ_{esc} . The average ($\langle \tau_{\text{esc}} \rangle$) and median ($\tilde{\tau}_{\text{esc}}$) escape times are evaluated at the end of each run.

Figure 3 shows the energy dependence of escape times. Blue and orange colors refer to the cases $\zeta \rightarrow \infty$ and $\zeta = 0$, respectively. We disregarded other cases ($\zeta = 10^{-2}, 10^{-4}$) displayed in Fig. 2 since, as expected, they show results analogous to the $\zeta = 0$ case. Blue and orange markers show the average escape times $\langle \tau_{\text{esc}} \rangle$, while light blue and orange markers display the median escape time $\tilde{\tau}_{\text{esc}}$. Blue and orange dashed lines indicate the average diffusive escape

time $\tau_D = L_{\text{esc}}^2/2D_{\text{iso}}$ (see, e.g., Eqs. (11) and (20-22) of Lipari (2014)), while light blue and orange dot-dashed lines display the prediction for the median diffusive escape time $\simeq 0.75\tau_D$, calculated from the distribution of Eqs. (20-21) in Lipari (2014). In both cases, the isotropic diffusion coefficient D_{iso} has been computed directly from simulations as in Figure 2.

Several interesting features emerge by inspecting Figure 3. At most energies, particle escape is well described by the diffusion approximation, as expected since $\lambda \ll L_{\text{esc}}$ (Fig. 2). The different diffusion properties recovered at low energies for decreasing ζ values reflect into a distinct energy dependence of the escape times. In the $\zeta \rightarrow \infty$ case, the escape time shows a trend close to $r_g^{-1/3}$, while in the FLRW-dominated scenario, the escape time becomes constant as the energy decreases.

At high enough energies the diffusive approximation eventually breaks down, and a transition to a ballistic escape is observed. For both $\zeta \rightarrow \infty$ and $\zeta = 0$, the median and average escape times saturate at two different values, respectively close to $\tilde{\tau}_{\text{esc},b} = 2L_{\text{esc}}/c$ (cerise-red dot-dashed) and $\langle \tau_{\text{esc},b} \rangle \simeq \frac{L_{\text{esc}}}{c} \ln\left(\frac{L_{\text{esc}}}{l_c}\right)$ (cerise-red dashed). Such a behavior can be interpreted as follows.

As we inject N_p particles isotropically, the number of particles moving with pitch angle $0 \leq \mu \leq 1$ is $n(\mu) = N_p/2$. These particles escape in a time $\tau \simeq L_{\text{esc}}/c\mu$. The number of particles with escape time between τ and $\tau + d\tau$ can be easily inferred as:

$$n(\tau) = \frac{N_p}{2} \frac{L_{\text{esc}}}{c\tau^2}. \quad (4)$$

The slope of the PDFs of $n(\tau)$ measured from numerical simulations is in agreement with the above $\simeq -2$ slope (not shown here). By requiring that the number of particles escaping with times $> \tau$ are half of the total number of particles with $\mu > 0$, i.e., $N_p/4$, it is easy to compute the median ballistic escape time $\tilde{\tau}_{\text{esc},b} = 2L_{\text{esc}}/c$. The average ballistic escape time is instead:

$$\langle \tau_{\text{esc},b} \rangle = \frac{\int_{\tau_{\text{min}}}^{\tau_{\text{max}}} d\tau n(\tau) \tau}{\int_{\tau_{\text{min}}}^{\tau_{\text{max}}} d\tau n(\tau)} \simeq \frac{L_{\text{esc}}}{c} \ln\left(\frac{c\tau_{\text{max}}}{L_{\text{esc}}}\right), \quad (5)$$

where $\tau_{\text{min}} = L_{\text{esc}}/c$ and $\tau_{\text{max}} \gg \tau_{\text{min}}$ is related to the particles with very small pitch-angle, μ_{min} , that spend a rather long time in the halo. We estimated μ_{min} by noticing that these particles perform a random walk deflecting by an angle $\Delta\theta \simeq \eta^{1/2}l_c/r_g$, where the number of scatterings is $\eta \simeq L_{\text{esc}}/(\mu l_c)$. When $\Delta\theta \sim L_{\text{esc}}/r_g$, i.e., $\mu_{\text{min}} \simeq l_c/L_{\text{esc}}$, these particles escape, thus providing $\tau_{\text{max}} \simeq L_{\text{esc}}^2/(c l_c)$ and $\langle \tau_{\text{esc},b} \rangle \simeq \frac{L_{\text{esc}}}{c} \ln\left(\frac{L_{\text{esc}}}{l_c}\right)$. This trend is shown in Figure 3 as a horizontal dash-dotted line and agrees well with the median escape time computed from simulations.

4 DISCUSSION

The recent accurate measurement of the spectra of primary and secondary nuclei and the detection of features in such spectra have brought up to surface the issue of the microphysics of CR scattering. At low energies CRs may be self-confined in the Galaxy (Amato & Blasi 2018), while at energies above a few hundred GeV self-confinement is inefficient and pre-existing turbulence is needed to scatter CRs. Such turbulence is unlikely to be Alfvénic (or slow magnetosonic) owing to the anisotropic cascade which provides little power at the resonant scales. Fast magnetosonic modes as a source of scattering may be also problematic due to the damping properties of these modes and the dependence of the spectrum upon plasma properties (Kempski & Quataert 2022).

We stress that all calculations highlighting problems in scattering high-energy particles refer to parallel diffusion: they start from a computation of the pitch-angle diffusion coefficient and use it to infer the spatial diffusion coefficient parallel to field lines. The hidden assumption is that the transport of CRs on Galactic scales is dominated by parallel diffusion. This is all but guaranteed, and in fact when parallel diffusion becomes ineffective, perpendicular diffusion remains in general at work. Aside from these considerations, the critical dependence of the amount of scattering at high energies upon environmental conditions casts some doubt on the fact that scattering in the traditional sense is actually playing a role in confining high-energy CRs. This doubt inspired the investigation discussed in the present article: if, because of either the anisotropic cascade of Alfvénic and slow magnetosonic modes or the damping of fast modes, the turbulence that affects particle motion were to remain confined around the injection scale, what would CR transport look like in the Galaxy?

Using numerical simulations of particle transport in synthetic turbulence made of a coherent field (bump in k space) changing orientation on scale l_c plus a power-law turbulent spectrum on smaller scales (larger values of k) with independent normalizations we showed that: 1) when the two components have comparable strength the propagation of CRs is diffusive with a diffusion coefficient in agreement with previous work (Subedi et al. 2017; Dundovic et al. 2020); 2) when the bump component is dominant, particles with low energies with respect to those resonating with perturbations in the bump diffuse with a pathlength comparable with the coherence scale $l_c \sim 30$ pc. 3) The pathlength associated with the resonant scattering depends on the normalization of the turbulence on such scales, if present. If at low energies CRs self-generate the turbulence on which they scatter, then this turbulence leads to a reduction of the diffusive pathlength, for those energies for which such a pathlength becomes $\lesssim l_c$. We estimated that this is expected to happen in the TeV region, tantalizingly close to the rigidity of the observed spectral breaks. Although we are not claiming that the transition occurs between resonant scattering on self-generated waves and FLRW, we think that this possibility is not excluded and that it deserves a dedicated investigation. It would certainly alleviate the need for fine tuning pointed out by Kempinski & Quataert (2022) and would make fast magnetosonic modes less indispensable at high energies.

We also exploited our numerical simulations for checking that the energy dependence of diffusion coefficients reflect in the CR confinement time in the Galaxy. The confinement time becomes energy independent at energies below ~ 30 PeV, while at higher energies there is a reduction $\propto E^{-2}$ (small-angle scattering) followed by another regime in which the confinement time is energy independent (ballistic propagation). A numerical simulation with a larger dynamical range would allow us to explore even lower energies, for which even small levels of resonant scattering would make the pathlength $< l_c$, thus newly introducing an energy dependence in the confinement time. Using the low energy diffusion coefficient derived from the observed B/C (or B/O) ratio, one can guess that the resonant scattering should become important for $E \lesssim$ TeV.

ACKNOWLEDGEMENTS

Test-particle simulations here presented have been performed on the Newton cluster at the University of Calabria (Italy). The authors thank A. Marcowith for reading a preliminary version of this manuscript and C. Evoli, O. Fornieri, and S.S. Cerri for fruitful discussion.

DATA AVAILABILITY

The data underlying this article will be shared on reasonable request to the corresponding author.

REFERENCES

Aguilar M., et al., 2015, *Phys. Rev. Lett.*, 115, 211101
 Aguilar M., et al., 2016, *Phys. Rev. Lett.*, 117, 231102
 Aguilar M., et al., 2017, *Phys. Rev. Lett.*, 119, 251101
 Amato E., Blasi P., 2018, *Adv. Space Res.*, 62, 2731
 Barnes A., 1966, *The Physics of Fluids*, 9, 1483
 Batchelor G. K., 1982, *The Theory of Homogeneous Turbulence*
 Blasi P., Amato E., Serpico P. D., 2012, *Phys. Rev. Lett.*, 109, 061101
 Casse F., Lemoine M., Pelletier G., 2001, *Physical Review D*, 65, 023002
 Chandran B. D. G., 2000, *Phys. Rev. Lett.*, 85, 4656
 Cho J., Lazarian A., 2002, *Phys. Rev. Lett.*, 88, 245001
 Cho J., Lazarian A., Vishniac E. T., 2002, *Astrophys. J.*, 564, 291
 Choutko V., 2016, in *Proceedings of The 34th International Cosmic Ray Conference — PoS(ICRC2015)*, p. 260, doi:10.22323/1.236.0260
 Chuchai P., Ruffolo D., Matthaeus W. H., Meechaj J., 2007, *Astrophys. J.*, 659, 1761
 Cohet R., Marcowith A., 2016, *Astronomy & Astrophysics*, 588, A73
 De Marco D., Blasi P., Stanev T., 2007, *J. Cosmol. Astropart. Phys.*, 2007, 027
 Dundovic A., Pezzi O., Blasi P., Evoli C., Matthaeus W. H., 2020, *Phys. Rev. D*, 102, 103016
 Evoli C., Morlino G., Blasi P., Aloisio R., 2020, *Phys. Rev. D*, 101, 023013
 Ferrière K., 2020, *Plasma Phys. Control. Fusion*, 62, 014014
 Fornieri O., Gaggero D., Cerri S. S., De La Torre Luque P., Gabici S., 2021, *Mon. Notices Royal Astron. Soc.*, 502, 5821
 Génolini Y., et al., 2017, *Phys. Rev. Lett.*, 119, 241101
 Goldreich P., Sridhar S., 1995, *Astrophys. J.*, 438, 763
 Holmes J. A., Scrima D. W., 1975, *Mon. Notices Royal Astron. Soc.*, 170, 251
 Kempinski P., Quataert E., 2022, *Mon. Notices Royal Astron. Soc.*, 514, 657
 Kuhlen M., Phan V. H. M., Mertsch P., 2022, *arXiv e-prints*, p. arXiv:2211.05882
 Kulsrud R., Pearce W. P., 1969, *Astrophys. J.*, 156, 445
 Lipari P., 2014, *arXiv e-prints*, p. arXiv:1407.5223
 Matthaeus W. H., Ghosh S., Oughton S., Roberts D. A., 1996, *J. Geophys. Res. Space Phys.*, 101, 7619
 Matthaeus W. H., Servidio S., Dmitruk P., Carbone V., Oughton S., Wan M., Osman K. T., 2012, *Astrophys. J.*, 750, 103
 Mertsch P., 2020, *Astrophys. Space Sci.*, 365, 135
 Oughton S., Matthaeus W. H., 2020, *Astrophys. J.*, 897, 37
 Pezzi O., Blasi P., Matthaeus W. H., 2022, *Astrophys. J.*, 928, 25
 Pucci F., Malara F., Perri S., Zimbardo G., Sorriso-Valvo L., Valentini F., 2016, *Mon. Notices Royal Astron. Soc.*, 459, 3395
 Reichherzer P., Becker Tjus J., Zweibel E. G., Merten L., Pueschel M. J., 2022, *Mon. Notices Royal Astron. Soc.*, 514, 2658
 Schekochihin A. A., 2022, *Journal of Plasma Physics*, 88, 155880501
 Shebhat J. V., Matthaeus W. H., Montgomery D., 1983, *J. Plasma Phys.*, 29, 525
 Skilling J., 1975, *Mon. Notices Royal Astron. Soc.*, 172, 557
 Sonsrettee W., Subedi P., Ruffolo D., Matthaeus W. H., Snodin A. P., Wongpan P., Chuchai P., 2015, *Astrophys. J.*, 798, 59
 Sonsrettee W., et al., 2016, *Astrophys. J. Suppl. Ser.*, 225, 20
 Sridhar S., Goldreich P., 1994, *Astrophys. J.*, 432, 612
 Subedi P., et al., 2017, *Astrophys. J.*, 837, 140
 Tomassetti N., 2012, *Astrophys. J. Lett.*, 752, L13
 Völk H. J., 1973, *Astrophys. Space Sci.*, 25, 471
 Yan H., Lazarian A., 2002, *Phys. Rev. Lett.*, 89, 281102
 Yan H., Lazarian A., 2008, *Astrophys. J.*, 673, 942
 Zhou Y., Matthaeus W. H., 1990, *J. Geophys. Res. Space Phys.*, 95, 14881

This paper has been typeset from a $\text{\TeX}/\text{\LaTeX}$ file prepared by the author.